



## Hydrological data assimilation with the ensemble Kalman filter: Use of streamflow observations to update states in a distributed hydrological model

Martyn P. Clark<sup>a,\*</sup>, David E. Rupp<sup>a,1</sup>, Ross A. Woods<sup>a</sup>, Xiaogu Zheng<sup>a</sup>, Richard P. Ibbitt<sup>a</sup>, Andrew G. Slater<sup>b</sup>, Jochen Schmidt<sup>a</sup>, Michael J. Uddstrom<sup>a</sup>

<sup>a</sup> National Institute for Water and Atmospheric Research (NIWA), 10 Kyle Street, Riccarton, Christchurch, New Zealand

<sup>b</sup> Cooperative Institute for Research in Environmental Sciences, University of Colorado, Boulder, CO 80309, USA

### ARTICLE INFO

#### Article history:

Received 9 August 2007

Received in revised form 9 June 2008

Accepted 12 June 2008

Available online 28 June 2008

#### Keywords:

Assimilation

Streamflow

Ensemble

### ABSTRACT

This paper describes an application of the ensemble Kalman filter (EnKF) in which streamflow observations are used to update states in a distributed hydrological model. We demonstrate that the standard implementation of the EnKF is inappropriate because of non-linear relationships between model states and observations. Transforming streamflow into log space before computing error covariances improves filter performance. We also demonstrate that model simulations improve when we use a variant of the EnKF that does not require perturbed observations. Our attempt to propagate information to neighbouring basins was unsuccessful, largely due to inadequacies in modelling the spatial variability of hydrological processes. New methods are needed to produce ensemble simulations that both reflect total model error and adequately simulate the spatial variability of hydrological states and fluxes.

© 2008 Elsevier Ltd. All rights reserved.

### 1. Introduction

The science of hydrological forecasting involves predicting future storages and fluxes of water in a river basin based on both the water stored in the basin at the start of the forecast and the external forcing to the basin during the forecast period. A great deal of recent research focuses on the use of numerical weather prediction model output to produce streamflow forecasts (e.g., [14,9,19,4]), but few studies evaluate the forecast improvements that are possible from improved estimates of basin states at the start of the forecast period [42].

Data assimilation can improve estimates of basin states and hence improve streamflow forecasts [42]. The basic idea of data assimilation is to quantify errors in both the hydrological model and observations, and update hydrological model states in a way that optimally combines model simulations with observations. Data assimilation has great potential in *distributed* hydrological models, both by improving state estimates at internal locations in a gauged river basin and by improving state estimates in ungauged basins. However, this potential seems largely unexploited [45]. The purpose of this paper is to discuss the issues involved with using streamflow observations to update states in a distributed hydrological model with the ensemble Kalman filter.

The remainder of this paper is organized as follows. We review alternative data assimilation methods in Section 2, and justify the selection of the ensemble Kalman filter method for this study. In Section 3 we describe the ensemble Kalman filter, and a variant, the ensemble square root Kalman filter. Section 4 describes methods for quantifying model error, and Section 5 describes methods for quantifying observation error. Section 6 describes application of the ensemble Kalman filter in a distributed hydrological model, including details of the model configuration, estimation of error parameters, and implementation of the ensemble Kalman filter (a detailed description of the hydrological model is provided in Appendix A). We discuss results in Section 7, including (i) the impact of assimilating streamflow observations at the basin outlet on streamflow simulations at interior points in the basin; (ii) the impact of assimilating streamflow at interior points on streamflow simulations at the basin outlet; and (iii) the potential to update hydrological states in ungauged basins. Finally, Section 8 summarizes results and explores implications for future work.

### 2. Review of data assimilation methods

Several methods can be used to assimilate data into hydrological models, each of which has strengths and weaknesses (e.g., [25]). The earliest method for hydrological data assimilation is an extension to the linear Kalman filter (e.g., [23,24,46,47]). In the extended Kalman filter the hydrological model is rendered in state-space form in which each model state is continuously differentiable with respect to all other model states. The estimate of model error at the

\* Corresponding author. Tel.: +64 3 343 7881.

E-mail address: [mp.clark@niwa.co.nz](mailto:mp.clark@niwa.co.nz) (M.P. Clark).

<sup>1</sup> Now at DHI Water and Environment, Inc., Portland, OR 97204, USA.

time of an observation is estimated by propagating the covariance matrix of model errors forward in time using a linearized model operator [23]. This approach is unstable in cases of strong model non-linearities [16,26]. Also, Reichle et al. [33] point out that application of the extended Kalman filter can be impossible for large-scale environmental assimilation problems (e.g., distributed hydrological models), unless approximations are made (e.g., ignoring spatial correlations among sub-catchments). However, such approximations limit the applicability of the extended Kalman filter, as knowledge of the spatial correlations between model states (e.g., soil moisture) and model fluxes at observing points in the basin (e.g., streamflow) is critical for updating hydrological states throughout the basin (see also [34]).

Another approach for hydrological data assimilation is variational methods (e.g., [32,36]). In hydrological applications of variational methods the model error is usually assumed to be temporally constant (e.g., [36]), and the problem reduces to identifying a set of model states that minimizes a cost function that defines differences between model states and observations. This is a (typically large) minimization problem, in which a linearized version of the hydrological model – the adjoint model – is used to compute the gradient of the cost function. The advantage of variational methods is that they do not forecast the model error covariance matrix and hence do not require a state-space formulation of the hydrological model required in the extended Kalman filter [36]. Variational methods do however require development of an adjoint model, which complicates implementation of the method.

Yet another approach to data assimilation is the ensemble Kalman filter. This method has recently gained popularity in hydrology, partly because increased computing power makes ensemble simulations feasible, and because it is easy to implement. In the ensemble Kalman filter (e.g., [17,18,42,45]) the hydrological model is run forward in time with a finite set of ensemble members, where each ensemble member is an equally-plausible representation of the real-world. Model error is then estimated directly from the ensemble by assuming that the ensemble mean is “truth” and computing the variance of the differences between each ensemble member and the ensemble mean (note, this assumes the ensemble is unbiased). As with other methods, the update to model states depends on the relative error in the model and observations, and the modelled covariance between model states and model fluxes at observing points in the basin. The advantages of the ensemble Kalman filter are that it does not require reformulation of the model into state-space form (as in the extended Kalman filter), and it does not require specification of the temporally constant model error covariance or development of a separate adjoint model (as in variational methods). The method does however require development of techniques to produce ensemble model simulations. Also, as with the extended Kalman filter and variational methods, the update to model states in the ensemble Kalman filter assumes the model errors have a Gaussian distribution – an assumption that rarely holds in hydrological models [27].

Another ensemble data assimilation method is the particle filter [29,2,27,43]. The particle filter differs from most other data assimilation methods in that the model states are not updated. Rather, each model ensemble member is assigned a probability (or weight) based on the difference between each ensemble member and the observations and the relative error in the model and observations. The probability distribution of model predictions can then be computed as a weighted combination of the ensemble members. The advantage of the particle filter is that it does not assume Gaussian model errors [27]. It does however require many more ensemble members than the ensemble Kalman filter to produce reliable estimates of model error [27,43].

The main reasons for selecting the ensemble Kalman filter for this study are because it is easy to implement and because the

need to construct model ensembles is consistent with our probabilistic approach to streamflow forecasting. The ensemble Kalman filter is used in preference to the particle filter because previous studies have shown that it requires fewer ensemble members (e.g., [43]).

### 3. Ensemble Kalman filters

#### 3.1. Ensemble Kalman filter (EnKF)

The basic idea of data assimilation is to quantify errors in both the hydrological model and observations, and update hydrological model states in a way that optimally combines model background (i.e., the model forecast at the time of the observations) with observations. In the ensemble Kalman filter (EnKF), model error estimates are produced by assuming that the ensemble mean is “truth” and computing the variance of the differences between each ensemble member and the ensemble mean. Each individual observation is then updated based on the relative error in both the model and observations.

The EnKF can be formalized as follows. Let  $\mathbf{X}^b$  be the  $nstate \times nens$  background matrix of model states, where  $nstate$  is the number of state variables and  $nens$  is the number of ensemble members, that is

$$\mathbf{X}^b = (\mathbf{x}_1^b, \dots, \mathbf{x}_{nens}^b) \quad (1a)$$

where  $\mathbf{x}_1^b, \dots, \mathbf{x}_{nens}^b$  are the background vectors of all model states for each of the  $nens$  ensemble members before the state update. The ensemble mean is defined as

$$\bar{\mathbf{x}}^b = \frac{1}{nens} \sum_{i=1}^{nens} \mathbf{x}_i^b \quad (1b)$$

The ensemble anomaly for the  $i$ th ensemble member is  $\mathbf{x}_i^a = \mathbf{x}_i^b - \bar{\mathbf{x}}^b$ , and the ensemble of anomalies is defined as

$$\mathbf{X}^a = (\mathbf{x}_1^a, \dots, \mathbf{x}_{nens}^a) \quad (1c)$$

An estimate of the model error covariance is then computed directly from the ensemble anomalies, as

$$\mathbf{P}^b = \frac{1}{nens - 1} \mathbf{X}^a \mathbf{X}^{aT} \quad (1d)$$

Having  $\mathbf{P}^b$  it is relatively straightforward to update model states. The update equation is

$$\mathbf{x}_i^a = \mathbf{x}_i^b + \mathbf{K}(\mathbf{y}_i - \mathbf{H}\mathbf{x}_i^b) \quad (2a)$$

where

$$\mathbf{K} = \mathbf{P}^b \mathbf{H}^T (\mathbf{H} \mathbf{P}^b \mathbf{H}^T + \mathbf{R})^{-1} \quad (2b)$$

Note that each ensemble member is updated separately Eq. (2a). In Eq. (2)  $\mathbf{x}_i^a$  is the analysis of model states after the update,  $\mathbf{y}_i$  is the  $nobs \times 1$  vector of “observations” ( $nobs$  is the number of observations),  $\mathbf{H}$  is the  $nobs \times nstate$  operator that converts the model states to observation space,  $\mathbf{K}$  is the Kalman gain, and  $\mathbf{R}$  is the  $nobs \times nobs$  observation error covariance matrix. In the usual implementation of the ensemble Kalman filter (e.g., [8,18]), the  $nobs$  elements of  $\mathbf{y}_i$  for each ensemble member are sampled from a distribution with mean equal to the observations and variance  $\mathbf{R}$ , providing  $nens$  vectors of observations that are used to update each of the  $nens$  ensemble members.

A key part of (2b) is the  $\mathbf{H}$  matrix used to map model states to observation states. In simple applications where the observed and modelled quantities are the same,  $\mathbf{H}$  is just a matrix of weights used to interpolate a gridded field to observation locations. In typical applications, a separate model (termed the forward model) is

used to compute the model equivalent of the observation from model states. For example, in meteorological data assimilation a radiative transfer model is used to compute the equivalent of satellite radiances from the temperature and water vapor predictions from the numerical weather prediction model. The forward model can be included directly in the  $\mathbf{H}$  matrix if it is linear; however, the forward model must be run separately if it is non-linear. If there is an exact match between observations and their model equivalent (i.e., from the forward model), the model state vector can be augmented with the model equivalent of the observation [18], and the  $nobs \times nstate$   $\mathbf{H}$  matrix can be constructed to have a value of 1 for elements where there is a model prediction of the observation, and 0 where there is no equivalent observation. In this case  $\mathbf{HP}^b\mathbf{H}^T$  is the  $nobs \times nobs$  matrix of model covariance at observing locations in the basin and  $\mathbf{P}^b\mathbf{H}^T$  is the  $nstate \times nobs$  matrix of covariance between modelled streamflow at observing locations in the basin and model states throughout the basin (Eq. (2b)). In our application with a distributed hydrological model, the same model is used to map inputs to states and map states to observations – the hydrological model therefore serves as the forward model. There is an exact match between observations and their model equivalent (streamflow at observing sites in the basin), so the  $\mathbf{H}$  matrix is just ones and zeroes as described above.

### 3.2. Ensemble square root filter (EnSRF)

The perturbed observations in the EnKF can have a detrimental effect in that they add noise to the analysis. Burgers et al. [8] demonstrated that perturbed observations are actually necessary in the standard implementation of the filter to provide the correct analysis error covariance (that is, the error after the assimilation, Eq. (2a)). The analysis error covariance is [8,44]

$$\mathbf{P}^a = (\mathbf{I} - \mathbf{KH})\mathbf{P}^b(\mathbf{I} - \mathbf{KH})^T + \overline{\mathbf{K}(\mathbf{y} - \mathbf{y}^t)(\mathbf{y} - \mathbf{y}^t)^T\mathbf{K}^T} \quad (3a)$$

Burgers et al. [8] demonstrated that if  $\overline{(\mathbf{y} - \mathbf{y}^t)(\mathbf{y} - \mathbf{y}^t)^T} = \mathbf{R}$ , then (since from Eq. (2b),  $\mathbf{K}(\mathbf{HP}^b\mathbf{H}^T + \mathbf{R}) = \mathbf{P}^b\mathbf{H}^T$ )

$$\begin{aligned} \mathbf{P}^a &= (\mathbf{I} - \mathbf{KH})\mathbf{P}^b(\mathbf{I} - \mathbf{KH})^T + \mathbf{KRK}^T \\ &= \mathbf{P}^b - \mathbf{KHP}^b - \mathbf{P}^b\mathbf{H}^T\mathbf{K}^T + \mathbf{K}(\mathbf{HP}^b\mathbf{H}^T + \mathbf{R})\mathbf{K}^T \\ &= (\mathbf{I} - \mathbf{KH})\mathbf{P}^b \end{aligned} \quad (3b)$$

but, in the case of when observations are not perturbed,  $\overline{(\mathbf{y} - \mathbf{y}^t)(\mathbf{y} - \mathbf{y}^t)^T} = \mathbf{0}$ , then Eq. (3a) simplifies to

$$\mathbf{P}^a = (\mathbf{I} - \mathbf{KH})\mathbf{P}^b(\mathbf{I} - \mathbf{KH})^T \quad (3c)$$

and the analysis error covariance is too low. Perturbed observations are therefore necessary.

Whitaker and Hamill [44] introduced the ensemble square root filter (EnSRF) that provides the correct analysis error covariance without perturbing the observations. The basic idea is to identify a modified Kalman gain  $\tilde{\mathbf{K}}$  such that

$$(\mathbf{I} - \tilde{\mathbf{K}}\mathbf{H})\mathbf{P}^b(\mathbf{I} - \tilde{\mathbf{K}}\mathbf{H})^T = (\mathbf{I} - \tilde{\mathbf{K}}\mathbf{H})\mathbf{P}^b \quad (3d)$$

The solution to this equation is [44]

$$\tilde{\mathbf{K}} = \mathbf{P}^b\mathbf{H}^T \left[ \left( \sqrt{\mathbf{HP}^b\mathbf{H}^T + \mathbf{R}} \right)^{-1} \right]^T \times \left[ \sqrt{\left( \mathbf{HP}^b\mathbf{H}^T + \mathbf{R} \right) + \sqrt{\mathbf{R}}} \right]^{-1} \quad (3e)$$

with update equations

$$\begin{aligned} \bar{\mathbf{x}}^a &= \bar{\mathbf{x}}^b + \mathbf{K}(\bar{\mathbf{y}} - \mathbf{H}\bar{\mathbf{x}}^b) \\ \mathbf{x}'^a &= \mathbf{x}'^b + \tilde{\mathbf{K}}(\mathbf{y}' - \mathbf{H}\mathbf{x}'^b) \end{aligned} \quad (3f)$$

where as before the ensemble mean is denoted by an overbar and the deviations from the ensemble mean are denoted by a prime.

Note that  $\mathbf{y}' = \mathbf{0}$  (no perturbed observations), and that the original Kalman gain is used to update the ensemble mean and the modified Kalman gain is used to update ensemble anomalies. Whitaker and Hamill [44] showed that the sampling error associated with perturbed observations makes the EnSRF more accurate than the EnKF for the same ensemble size.

## 4. Quantifying model error

The ensemble Kalman filter uses the variance between multiple ensemble members to quantify model error. Ensembles are produced by stochastically perturbing the precipitation forcing and model states (in this study, soil moisture and aquifer storage). These perturbations account for uncertainties in model inputs as well as some of the uncertainty in the model itself (uncertainty in model parameters and model structure).

### 4.1. Perturbations to model inputs and states

Ensembles of precipitation forcing are generated by

$$p' = p\varphi_p \quad (4a)$$

The precipitation multiplier  $\varphi_p$  is given as

$$\varphi_p = (1 - \varepsilon_p) + 2u_p\varepsilon_p \quad (4b)$$

where  $u_p$  is a uniform random number, such that  $\varphi_p$  is a realization from a uniform distribution ranging from  $1 - \varepsilon_p$  to  $1 + \varepsilon_p$ .

Soil moisture is perturbed as

$$S'_r = S_r + \varphi_s \quad (5a)$$

The coefficient  $\varphi_s$  is parameterized as a function of the absolute change in soil moisture between the start of the time step  $S_r(t - 1)$  and the end of the time step  $S_r(t)$  by

$$\varphi_s = -\varepsilon_s|S_r(t) - S_r(t - 1)| + 2u_s\varepsilon_s|S_r(t) - S_r(t - 1)| \quad (5b)$$

where  $u_s$  is a uniform random number, such that  $\varphi_s$  is a realization from a uniform distribution ranging from  $-\varepsilon_s|S_r(t) - S_r(t - 1)|$  to  $\varepsilon_s|S_r(t) - S_r(t - 1)|$ .

Aquifer storage, as represented by the depth to the water table ( $\bar{z}$ ) is perturbed as

$$\bar{z}' = -m \left\{ \ln \left[ \frac{(q_b + \phi_z)}{K_0 m} \right] + \lambda \right\} \quad (6a)$$

Here the depth to the water table ( $\bar{z}$ ) is modified by adding noise to baseflow ( $q_b$ ) and inverting the baseflow equation (see Appendix A on model description for definition of terms). This parameterization is somewhat model-specific, but in principle most baseflow equations can be inverted. The perturbations are parameterized in terms of baseflow only (instead of the time change in the depth to the water table) because drainage from the root zone to the aquifer is already modified by perturbations to soil storage (again, see Appendix A for model description). The coefficient  $\varphi_z$  is estimated as

$$\varphi_z = -\varepsilon_z q_b + 2u_z\varepsilon_z q_b \quad (6b)$$

where  $u_z$  is a uniform random number, such that  $\varphi_z$  is a realization from a uniform distribution ranging from  $-\varepsilon_z q_b$  to  $\varepsilon_z q_b$ .

Our approach of perturbing model states differs from the traditional approach where perturbations are temporally constant (e.g., [33,13]). Parameterizing model errors in terms of the time change in model states means that perturbations will be small when model fluxes are small (e.g., inter-storm periods) and perturbations will be large when model fluxes are large (e.g., storm periods). This approach will not account for model errors that arise when large fluxes of water are inadequately simulated (or missed) by the model. However, we believe that imposing time variant model errors in

this way is more representative of model uncertainty than imposing temporally constant model errors.

The parameters required for perturbing model states are therefore fractional error parameters for precipitation ( $\epsilon_p$ ), soil moisture ( $\epsilon_s$ ) and aquifer storage ( $\epsilon_z$ ).

#### 4.2. Space–time correlation of model errors

The uniform random numbers  $u_p$ ,  $u_s$  and  $u_z$  in Eqs. (4–6) should be correlated in both space and time. Following Evensen [18], the time evolution of model errors is simulated as

$$\mathbf{s}_t = \rho \mathbf{s}_{t-1} + \sqrt{1 - \rho^2} \mathbf{w}_{t-1} \quad (7a)$$

where  $\mathbf{w}_{t-1}$  is a  $ncat \times 1$  vector of spatially correlated Normally distributed random numbers with mean equal to zero and variance equal to 1 ( $ncat$  is the number of sub-catchments in the basin). The coefficient  $\rho$  determines the temporal correlation of the stochastic forcing, where  $\rho = 0$  generates a sequence of white noise and  $\rho = 1$  will remove the stochastic forcing and represent the model errors with a random field that is constant in time [18].

The random fields  $\mathbf{s}_t$  are transformed to uniform distributions required in Eqs. (4–6) by computing the cumulative probability of a standard normal deviate

$$\mathbf{u}_t = \frac{1}{2} \operatorname{erfc}\left(\frac{\mathbf{s}_t}{\sqrt{2}}\right) \quad (7b)$$

where  $\operatorname{erfc}()$  is the complementary error function, and  $\mathbf{u}$  ranges from zero to one. We elect to use uniform distributions for all stochastic perturbations, partly for simplicity, partly because we have no knowledge of the appropriate distribution to use, and partly because truncated distributions do not result in large random perturbations and unrealistic results.

The temporal persistence parameter in Eq. (7a),  $\rho$ , can be expressed in terms of decorrelation time,  $\tau$

$$\rho = 1 - \frac{\Delta t}{\tau} \quad (7c)$$

where  $\Delta t$  is the length of the model time step.

The spatially correlated field  $\mathbf{w}$  is generated assuming an isotropic correlation structure that decays exponentially as a function of distance

$$r_{ij} = \exp\left(-\frac{d_{ij}}{L}\right) \quad (7d)$$

where  $r_{ij}$  is the correlation between point  $i$  and  $j$ ,  $d_{ij}$  is the distance between point  $i$  and  $j$ , and  $L$  is the correlation length scale. The matrix decomposition method outlined by Clark and Slater [10] is used to generate  $\mathbf{w}$ .

The parameters required to simulate the time evolution of model errors are therefore  $\tau$ , which defines the decorrelation time, and  $L$ , which defines the correlation length scale. These parameters are required for precipitation, soil moisture, and aquifer storage.

### 5. Quantifying observation errors

Quantifying observation errors is important as the error in the observation (relative to the error in the model) determines the weight assigned to the observation when it is assimilated into a model. Errors in streamflow stem both from measurement errors in water level (stage) and uncertainties in the rating curve that is used to transform measurements of stage to estimates of streamflow. Sorooshian and Dracup [38] point out that the concavity in the stage–discharge relationship means that the errors in measurement of stage translate into higher errors in discharge at high stage levels than at low stage levels (see also Fig. 3). The uncertainties at

high stage levels are also larger because of fewer gaugings of high flows and subsequent large uncertainty in the rating curves at high water levels. For this study we parameterize errors in streamflow measurements  $\sigma_{\text{obs}}^2$  as a function of the streamflow observation  $q_{\text{obs}}$

$$\sigma_{\text{obs}}^2 = (\epsilon_{\text{obs}} q_{\text{obs}})^2 \quad (8)$$

where  $\epsilon_{\text{obs}}$  is a parameter that must be specified.

### 6. Application in a distributed hydrological model

The ensemble Kalman filter is applied in a distributed hydrological model (TopNet) in the Wairau river basin in New Zealand to test the capabilities of the approach and identify potential problems. The following sections provide a description of the model and basin (including model calibration methods), as well as details on specifying error parameters and implementing the ensemble Kalman filter.

#### 6.1. Model description

The distributed hydrological model TopNet has two fundamental components: (i) simulating the water balance over a number of sub-catchments throughout a river basin, and (ii) routing streamflow from each sub-catchment to the basin outlet. The water balance model includes simulating the storages and fluxes of water in the canopy, snowpack, unsaturated and saturated soil zone (Fig. 1). It also accounts for time delay in runoff of water within each sub-basin. Runoff from each sub-basin flows into a digital stream network and is routed to the basin outlet. A detailed description of TopNet is provided in Appendix A. Bandaragoda et al. [3] describe an earlier version of TopNet and its application in a distributed model intercomparison experiment.

TopNet requires a set of parameters to describe basin geometry, water holding capacity of the vegetation and soil, and the transmissibility of the subsurface in each sub-catchment (Table 1). Frequency distributions of the topographic wetness index and distance to streams are required for all catchments. These parameters are used for modelling sub-catchment variations in soil water balance and water routing to the stream network, and are calculated from a 30 m digital elevation model. Average soil and land cover parameters for each sub-catchment (Table 1) were generated by intersecting the sub-catchment polygon coverages with polygons from soils and land cover databases. The resulting intersection tables indicate the percentage of soils and land cover types per sub-catchment and can be used to calculate the mean values of soil/cover parameters, which are linked as look-up tables to soil/cover types. There is no *a priori* information for some TopNet parameters (e.g., recession constants, such as the Topmodel  $m$  parameter), and these parameters are set to constant values for all sub-catchments.

The network component of TopNet requires the digital topology of the river network and parameters for each reach of the network (Table 2), both of which were extracted from digital elevation models.

TopNet has a similar level of complexity to a range of existing hydrological models (e.g., [3,31]). As with any model it is necessary to make a number of simplifying assumptions in order to aggregate the storage of water that occurs in nature into control volumes (state variables) that we can manipulate on a computer, and to parameterize the fluxes of water between state variables. Without more extensive evaluation of the appropriateness of individual model components for the Wairau River basin (for example, using the method proposed by Clark et al. [12]), we have no *a priori* expectations of whether TopNet models will perform better or worse than other models.

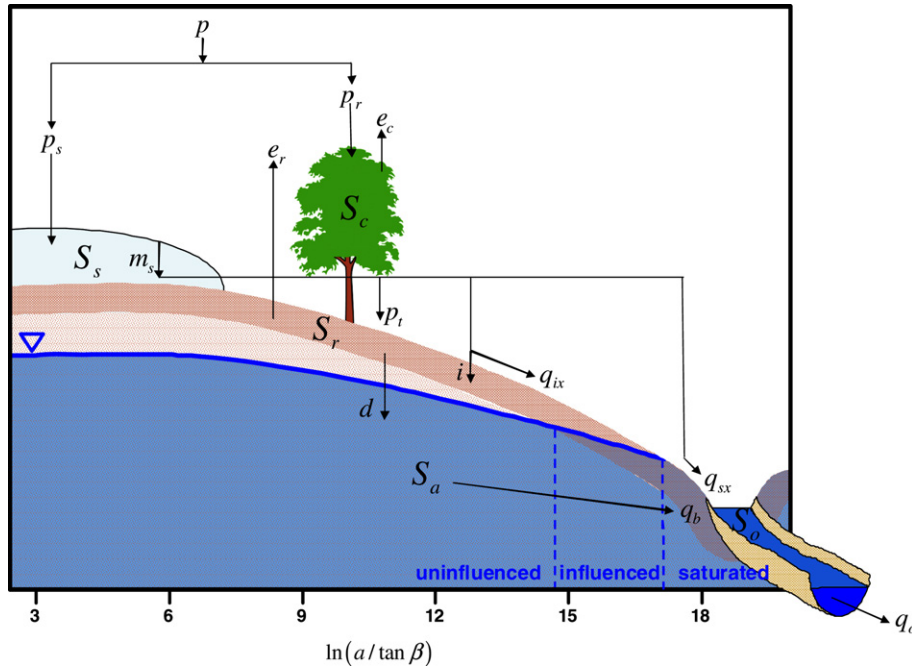


**Fig. 1.** Wiring diagram of catchment processes in the TopNet model. The topographic index  $\ln(a/\tan\beta)$  increases towards the stream indicating areas of topographic convergence and areas where the water table intersects the soil zone. The state variables and fluxes are defined in Appendix A.

**Table 1**  
Parameters of the basin model component of TopNet

Parameter	Symbol [units]	Description	Default value	Data source
Albedo	$\alpha$		–	LCDB <sup>c</sup>
Atmospheric lapse rate	$\gamma$ [K m <sup>-1</sup> ]		0.0065	Uniform
Wetness index (frequency distribution)	$\kappa_i$		–	REC <sup>a</sup>
Stream distance (frequency distribution)	$x_i$		–	REC <sup>a</sup>
Saturated store sensitivity	$m$ [m]	Describes exponential decrease of conductivity with depth	0.08	Uniform
Saturated hydraulic conductivity	$K_0$ [m s <sup>-1</sup> ]		0.01	Uniform
Drainable soil water	$\theta_{dr}$	Range between saturation and field capacity	–	LRI <sup>b</sup>
Plant-available soil water	$\theta_{pa}$	Range between field capacity and wilting point	–	LRI <sup>b</sup>
Depth of soil	$z_r$ [m]		–	LRI <sup>b</sup>
Exponent in drainage function	$c$	Describes drainage into saturated zone	–	LRI <sup>b</sup>
Wetting front suction	$\psi_f$ [m]	Parameter of Green–Ampt Infiltration capacity	0.3	Uniform
Overland flow velocity	$v$ [m s <sup>-1</sup> ]		0.1	Uniform
Canopy capacity	$C_c$ [m]		–	LCDB <sup>c</sup>
Evaporation enhancement	$c_r$	Increasing evaporation losses from interception	–	LCDB <sup>c</sup>

<sup>a</sup> The REC is the New Zealand River Environment Classification [37], which has spatial information about the river network and the catchments of New Zealand’s rivers. The REC includes a digital network of approximately 600,000 river reaches and related sub-basins for New Zealand. Topographic reach and catchment properties in the REC were derived from a 30 m digital elevation model (DEM).

<sup>b</sup> The LRI is the New Zealand Land Resource Inventory [28], which includes data on soils for all of New Zealand. The drainable water ( $\theta_{dr}$ ), the plant-available water ( $\theta_{pa}$ ) and the soil depth ( $z_r$ ) are obtained from look-up tables based on soil type, and the exponent in the drainage function ( $c$ ) is estimated as an empirical function of field capacity.

<sup>c</sup> The LCDB is the New Zealand land cover database, which includes land cover information for all of New Zealand. Albedo and vegetation parameters are obtained from look-up tables based on vegetation type (see [3] for more details).

**Table 2**  
Parameters of the network model component of TopNet

Model parameter	Symbol	Description	Data source
Network topology			REC
Reach length	$L$		REC
Reach slope	$S$		REC
Upstream area	$A$	Total upstream area above stream reach	REC
Reach Manning’s $n$	$N$		Uniform
Hydraulic geometry parameters	$a, b$	Relationship between drainage area and channel width $W = aA^b$	Uniform

We elect to use TopNet for this study for two main reasons. First, as detailed in Appendix A, TopNet is comprehensive enough to be suitable for use in a diverse range of river basins (i.e., the model includes vegetation and snow modules, it computes both infiltration-excess and saturation-excess runoff, and it simulates interactions between the water table and the soil zone). Ibbitt et al. [21] used TopNet to simulate streamflow in 14 different river basins across New Zealand in different climate regimes, and demonstrated that TopNet has medium ( $r^2 = 70\text{--}80\%$ ) and good accuracy ( $r^2 = 80\text{--}90\%$ ) in 10 out of the 14 river basins studied. We wished to use a model that is of comparable complexity to existing hydrological models that are used operationally for streamflow forecasting around the world. The similarities in structure between

TopNet and other models [31,12] imply that the results in this paper are relevant for other model structures. Our second reason for using TopNet is more pragmatic. TopNet was developed at the National Institute of Water and Atmospheric Research (NIWA), and our intimate knowledge of the model source code (and the modular model structure) means that it is relatively straightforward to add new modelling capabilities. Moreover, TopNet is the hydrological component of a nationwide flood forecasting system developed for New Zealand [11], so any new capabilities are immediately available for use as part of NIWA's flood forecasting service.

## 6.2. Site location and data

All model simulations are performed for the Wairau River basin in the northern South Island, New Zealand (Fig. 2). The Wairau drains an area of 3825 km<sup>2</sup>, and elevations in the catchment range from sea level to 2309 m. Vegetation in the Wairau includes pasture throughout the southern hills, native ever-green beech forest in the mountains to the west and southwest, a mix of native beech forest and exotic pine forest on the northern ranges, and vineyards on the Wairau plains (Fig. 2). The Wairau River is a braided gravel-bed river that is approximately 100 m wide in the lower reaches. Rainfall in the Wairau is lowest over the Wairau plains and southern hills (600 mm/year) and highest over the western ranges (5000 mm/year). There is a small hydropower scheme in the middle reaches of the Wairau and some irrigation on the Wairau plains, but the power generation and irrigation have only minor effects on catchment streamflow.

Model simulations were forced using interpolated climate data produced by Tait et al. [40] based on data from over 500 climate stations in New Zealand. Tait et al. [40] used a second-order derivative thin plate smoothing spline to interpolate point precipitation data across a regular 0.05° latitude–longitude grid (approx. 5 km × 5 km). Similar methods were used to interpolate point station data on daily maximum and minimum temperature, relative humidity, solar radiation, and wind speed to the same 0.05° latitude–longitude grid. Gridded time series for all climate variables have been produced for the period 1971–present. The interpolated climate data are used in TopNet by using data from the closest grid point to each sub-catchment as model forcing for that sub-catchment.

Model simulations are performed at hourly time steps, which requires temporal disaggregation of the daily gridded climate estimates. Temporal disaggregation of precipitation data was done by matching the temporal pattern of rainfall observed at hourly rain gauges in and around the Wairau catchment – hourly data were expressed as ratios of daily totals, the ratios were interpolated to the 0.05° grid, and the interpolated ratios were used to disaggre-

gate the daily gridded precipitation estimate. This approach is superior to interpolating the hourly precipitation data directly, both because there are many more daily rain gauges than hourly gauges, and because the daily precipitation data is less “noisy” than hourly precipitation data. Hourly temperature data was produced by fitting a sine curve to the spatially interpolated maximum and minimum temperatures, in which the time of maximum temperature was determined by fitting the parameters of the sine curve to hourly station data. Relative humidity data was temporally disaggregated by converting relative humidity to dew-point temperature, uniformly disaggregating the dew-point temperature for each hour in the day, and using the disaggregated temperature data to convert the hourly dew-point data to hourly estimates of relative humidity. Solar radiation was disaggregated by computing the daily atmospheric transmissivity (by dividing the interpolated solar radiation by estimates of clear-sky solar radiation), and using the daily transmissivity to modify hourly estimates of clear-sky radiation. Finally, wind speed was disaggregated uniformly throughout the day.

## 6.3. Model calibration

The default TopNet parameters (Table 1) were adjusted to improve the correspondence between model simulations and observations. Our calibration strategy for this study is to adjust the default TopNet model parameters (which vary spatially within the river basin) uniformly throughout the river basin using a spatially constant set of parameter multipliers, with the objective of minimizing errors at the basin outlet (Barnetts Bank). In this approach all sub-catchments receive the same multiplier. Data from interior sites were not used for model calibration. The use of a spatially constant set of parameter multipliers assumes that the spatial distribution of default TopNet parameters is suitable, which may be unrealistic in cases where the default parameters are spatially uniform (Table 1). Nevertheless, use of a single set of parameter multipliers for the entire basin reduces the dimensionality of the parameter estimation problem. Optimal parameter multipliers were obtained using the dynamically dimensioned search algorithm [41].

## 6.4. Model error parameters

Table 3 summarizes the model error parameters necessary to produce the ensemble simulations used in this study. The fractional error parameters  $\varepsilon_p$ ,  $\varepsilon_s$ , and  $\varepsilon_z$  should vary depending on both the model that is used and the basin that is modelled. Various combinations of the fractional error parameters were evaluated in an attempt to identify the set of error parameters that produces ensemble streamflow simulations with the correct ensemble

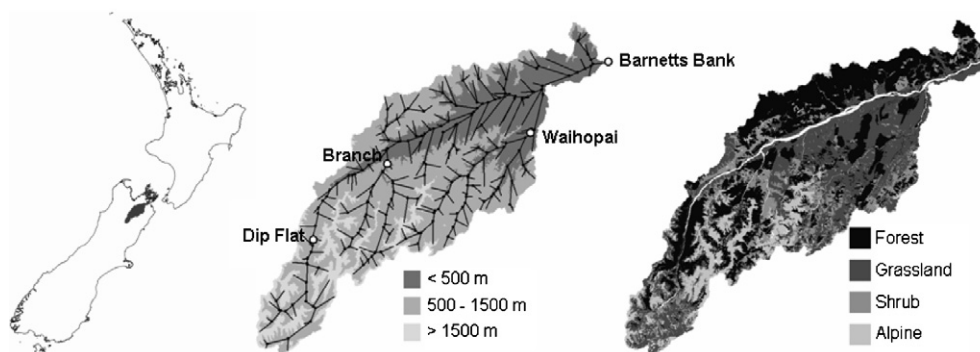


Fig. 2. The Wairau River basin, showing (left) location; (middle) elevation, digital river network, and location of observing sites; and (right) land cover. For TopNet simulations the Wairau basin is disaggregated into 380 sub-catchments, linked with the digital river network (middle).

**Table 3**  
Model error parameters

Model parameter	Symbol	Precipitation	Soil storage	Aquifer storage
Correlation length scale	$L$	100 km	100 km	100 km
Decorrelation time	$\tau$	1 day <sup>a</sup>	5 days	computed
Fractional error	$\varepsilon$	0.20	0.10	0.05

<sup>a</sup> Ensembles of daily precipitation were produced assuming there is no temporal persistence from one day to the next. Each ensemble member was then disaggregated to hourly intervals in exactly the same way (that is, each ensemble member has an identical temporal pattern of precipitation throughout the day, but different daily totals).

spread. However, there is high correlation between the different fractional error parameters. Large ensemble spread can be generated through large perturbations to precipitation, soil storage, or the depth to the water table, and it is difficult to disaggregate total error into the component parts based on streamflow observations alone (see also the discussion in [13]). In this study we specified fractional error parameters as  $\varepsilon_p = 0.20$ ,  $\varepsilon_s = 0.10$ , and  $\varepsilon_z = 0.05$  (Table 3). Note that for data assimilation it is preferable to over-estimate model errors rather than under-estimate them, as under-estimation of model errors can result in too much reliance on the model and filter divergence [13].

The correlation length scale  $L$  is set to 100 km for all variables. One hundred kilometer is approximately equal to the maximum width of the Wairau basin, or half its length. While this length scale may be appropriate for precipitation (e.g., [10]), there is very little

guidance on appropriate length scales for errors in soil moisture and aquifer storage. We will return to this issue later in the paper.

The decorrelation time  $\tau$  is specified at different values for precipitation, soil moisture, and aquifer storage.  $\tau$  is specified as one day for precipitation. The precipitation ensembles are constructed by perturbing the *daily* gridded precipitation estimates, and each ensemble member is then disaggregated to hourly intervals using the same method for each ensemble member; hence, the decorrelation time of one day implies there is no temporal persistence in precipitation from one day to the next. The decorrelation time for soil storage is specified at 5 days to reflect the relatively fast drainage of root zone soil water.

The decorrelation time for aquifer storage is estimated based on the drainage properties of the aquifer. Ambrose et al. [1] give baseflow recession curves for a linear reservoir as

$$q_b = q_s \exp\left(-\frac{\tau q_0}{m}\right) \tag{9a}$$

where  $q_b$  is baseflow,  $q_s$  is baseflow at a specified time,  $\tau$  is the time between  $q_b$  and  $q_s$ ,  $q_0$  is the baseflow at saturation (i.e., when  $\bar{z} = 0$ ), and  $m$  describes the decrease in hydraulic conductivity with depth and the depth scale of the aquifer. The linear reservoir has the convenient property that  $\tau$  can be expressed as a function of  $q_b/q_s$ . Given

$$q_0 = K_0 m e^{-\lambda} \tag{9b}$$

where  $K_0$  is the saturated hydraulic conductivity and  $\lambda$  is the mean topographic index (see Appendix A), and substituting (9b) in (9a), (9a) can be solved for  $\tau$  as

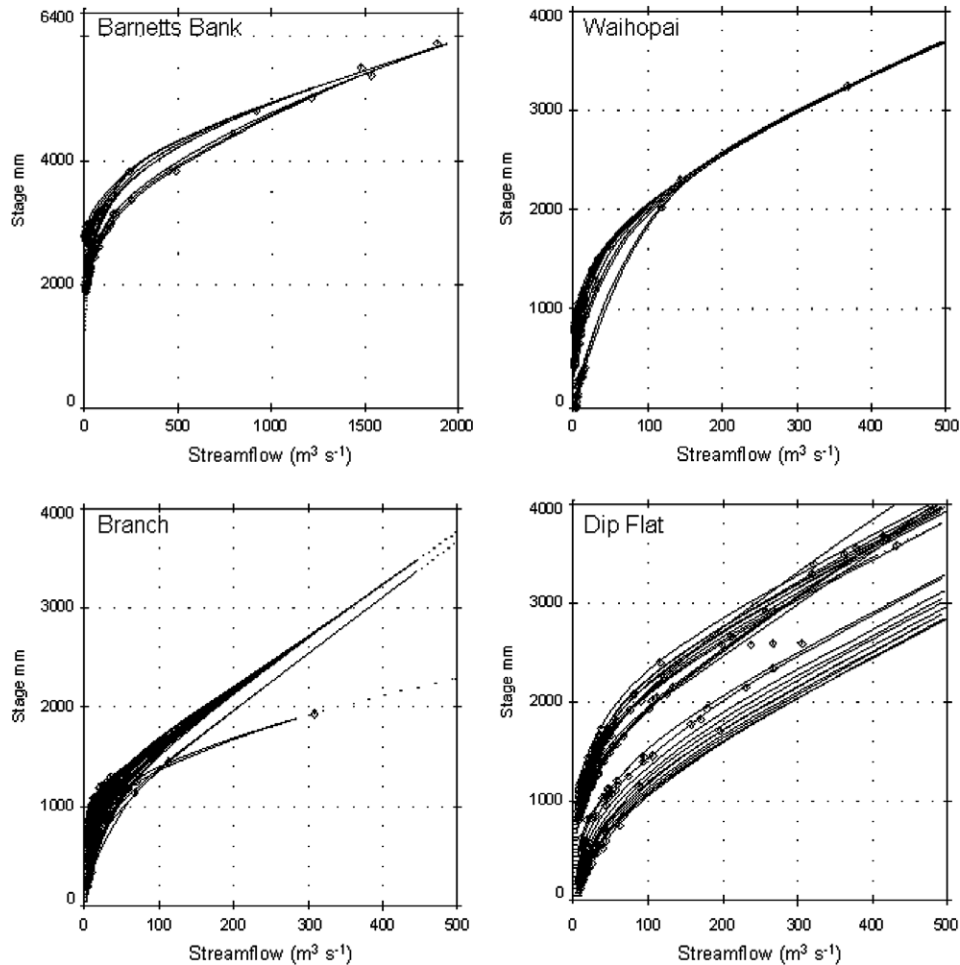


Fig. 3. Gaugings and rating curves for the four water level sites used in this study. See Fig. 2 for station locations.

$$\tau = \frac{\ln\left(\frac{q_b}{q_s}\right)}{K_0 e^{-\lambda}} \quad (9c)$$

In this study we specify  $q_b/q_s = 0.01$ , meaning  $\tau$  is the time required to reduce baseflow by two orders of magnitude. The decorrelation time for aquifer storage therefore differs based on the topographical characteristics and drainage parameters assigned to each sub-catchment – low values of  $\tau$  will be assigned to steep sub-catchments with short hillslope lengths, and to sub-catchments with high values of  $K_0$ .

### 6.5. Observation error parameters

Fig. 3 shows the gaugings and the rating curves for the four observing sites used in this study. Note that there is considerable scatter in the stage-streamflow relationships. The scatter occurs because movement of gravel in the stream bed changes the cross-section of the river at the measurement sites. Frequent gaugings are necessary in these gravel-bed rivers to identify changes in the cross-section of the river and associated changes in the rating curves.

The spread of ratings is not always a surrogate for uncertainty. For example, the convergence of the rating curves at high stage for Barnetts Bank and Waihopai occurs because all rating curves pass through the same high flow data point. The similarity between rating curves at high flows therefore reflect more a lack of data (gaugings) at high stage than high certainty in the stage-discharge relationship.

As outlined in Section 5 (Eq. (8)), errors in streamflow measurements depend on the streamflow rate. The error parameter is specified as  $\varepsilon_{\text{obs}} = 0.1$  for all four observing sites. Further, the measurement errors in stage and the uncertainties in the rating curves are assumed to be independent between sites (i.e., the matrix  $\mathbf{R}$  in Eqs. (2)–(3) is diagonal).

### 6.6. EnKF implementation

In this study our state vectors ( $\mathbf{x}_1^b, \dots, \mathbf{x}_{\text{nens}}^b$ ) used for data assimilation include soil storage, aquifer storage and surface storage for all sub-catchments in the basin, and model predictions of streamflow at observing locations in the basin. The model predictions of streamflow are actually diagnostic variables not state variables – they are the weighted average of flow particles that exit an observed reach in a given time step (see Appendix A) – and are not updated as part of the assimilation. While for some applications it may be desirable to update streamflow in the river network, computing covariances between network states is difficult because flow particles are at irregular times, so network states are not updated. The only variables updated are therefore the timestep-average state variables in model sub-basins.

The dimension of the matrices used for data assimilation is determined by the number of observation locations. Recall from Eq. (2) that  $\mathbf{HP}^b\mathbf{H}^T$  is the  $\text{nobs} \times \text{nobs}$  matrix of covariance between the model predictions of the observations and  $\mathbf{P}^b\mathbf{H}^T$  is  $\text{nstate} \times \text{nobs}$  the covariance between model predictions of the observations and model states. It is therefore never necessary to assemble the entire model error covariance matrix ( $\mathbf{P}^b$ ), which can be large in distributed models (multiple state variables for hundreds of sub-catchments). An efficient method for implementing the EnKF is as follows:

(loop through time)

1. Perturb precipitation inputs and model states.
2. Run the model for each ensemble member until a new observation becomes available (in this case one time step of length one hour).

3. Identify all observing sites in the basin with valid data (*nobs*), and assemble the *nobs* observation vector  $\mathbf{y}$  and the  $\text{nobs} \times \text{nobs}$  observation error matrix  $\mathbf{R}$ . Methods to define observation error are explained in Section 5.
4. Compute the  $\text{nobs} \times \text{nobs}$  model error covariance matrix  $\mathbf{HP}^b\mathbf{H}^T$ , that describes covariance between model predictions of the observations.
5. Compute  $(\mathbf{HP}^b\mathbf{H}^T + \mathbf{R})^{-1}$

(loop through unobserved model states)

6. Assemble the  $\text{nobs} + 1 \times \text{nens}$  state matrix  $\mathbf{X}^b = (\mathbf{x}_1^b, \dots, \mathbf{x}_{\text{nens}}^b)$ , where the “extra” row is the unobserved model state. Note that the dimension of  $\mathbf{X}^b$  is  $\text{nobs} + 1 \times \text{nens}$ , instead of  $\text{nstate} \times \text{nens}$ , because we are only processing one unobserved model state at a time.
7. Compute the  $\text{nobs} + 1 \times \text{nobs}$  matrix  $\mathbf{P}^b\mathbf{H}^T$ . The elements of  $\mathbf{P}^b\mathbf{H}^T$  that correspond to observations are taken directly from  $\mathbf{HP}^b\mathbf{H}^T$  (computed in step 4), and are not re-computed here.
8. Compute the Kalman gain,  $\mathbf{K} = \mathbf{P}^b\mathbf{H}^T(\mathbf{HP}^b\mathbf{H}^T + \mathbf{R})^{-1}$

(loop through model ensemble members)

9. Perturb observations,  $\mathbf{y}_i = \mathbf{y} + \boldsymbol{\zeta}$ ,  $\boldsymbol{\zeta} \sim N(0, \mathbf{R})$
10. Compute the  $\text{nobs} + 1 \times 1$  update vector,  $\mathbf{v}_i = \mathbf{K}(\mathbf{y}_i - \mathbf{H}\mathbf{x}_i^b)$
11. Update the unobserved state,  $x_{\text{nobs}+1,i}^a = x_{\text{nobs}+1,i}^b + v_{\text{nobs}+1,i}$  (note we are processing one state variable at a time, so  $x$  and  $v$  are scalars).
12. Check for physical realism, i.e., storages are not negative or greater than capacity, and make appropriate corrections

(end looping through ensemble members)

(end looping through unobserved model states)

(end looping through time)

The EnSRF is implemented using the same method, with all matrix square roots and inverses computed in step 5 before looping through unobserved model states. Implementing the EnSRF only involves computing the square root of matrices that are of dimension  $\text{nobs} \times \text{nobs}$ , which, for the case of assimilating streamflow observations, does not impose a significant computational cost (there are less than 10 operational water level recorders in most river basins in New Zealand).

## 7. Results and discussion

Ensemble simulations were run for the period 8th June–3rd July 2002 to illustrate the behaviour of the ensemble Kalman filter. Fig. 4 shows results from four simulations: (a) the control simulation (no data assimilation); (b) the standard implementation of the EnKF; (c) the EnKF, but with modelled and observed streamflow transformed to log space before computing the Kalman gain; and (d) the EnSRF in log space. It is immediately apparent that the standard implementation of the EnKF (Fig. 4b) results in somewhat erratic streamflow simulations. This occurs because relationships between streamflow and model states are non-linear, and, consequently, state updates are exceptionally large in situations where modelled streamflow is much higher than observed streamflow. The performance of the Kalman filter is significantly improved when streamflow is transformed to log space prior to computing the Kalman gain (Fig. 4c). Note also that the log EnSRF performs slightly better than the log EnKF (Fig. 4d), and is used in the remainder of the paper.

It is possible that assimilating data at the basin outlet will improve streamflow simulations at interior locations in the basin,

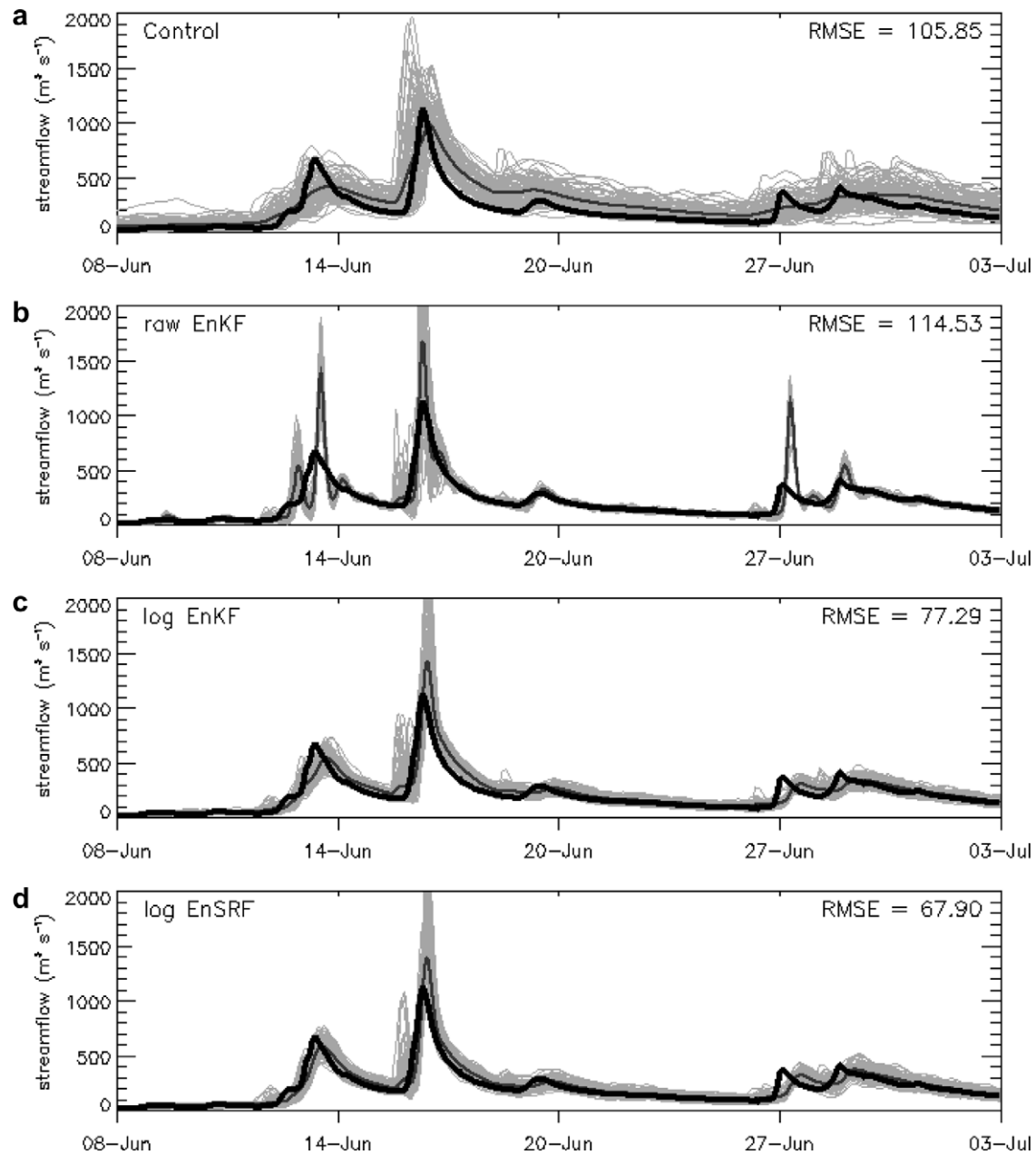


**Fig. 4.** Ensemble simulations for the Wairau at Barnett's Bank for (a) the control simulation (no data assimilation); (b) the standard implementation of the EnKF, but with modelled and observed streamflow transformed to log space before computing the Kalman gain; and (c) the EnKF, but with modelled and observed streamflow transformed to log space before computing the Kalman gain; and (d) the EnSRF in log space. The light grey lines are individual ensemble members, the grey line is the ensemble mean, and the thick black line is observations. In these simulations data was only assimilated at Barnett's Bank.

and, similarly, that assimilating data at internal locations will improve streamflow simulations at the basin outlet. To test these ideas, Fig. 5 illustrates streamflow simulations for (a) the control run (no data assimilation), (b) simulations where data is only assimilated at the outlet (Barnett's Bank); and (c) simulations where data is only assimilated at interior locations (Waihopai at Craigloch, Branch at Weir Intake, and Wairau at Dip Flat). Recall that data from interior locations was not used for model calibration.

Fig. 5 (middle column) shows that the RMSE of streamflow simulations at interior locations are actually degraded when data is only assimilated at the outlet. This is not entirely surprising. The state updates at interior locations depend on both the difference between model simulations and observations at the outlet, and the covariance between model states and the model equivalent

of the observations. Hence, model simulations at interior locations will only improve if the time series of errors at interior locations is similar to the time series of errors at the basin outlet. Consider for example the streamflow simulations on around 14th June for Branch at Weir Intake. In the control run streamflow is over-estimated at Barnett's Bank but under-estimated at Branch at Weir Intake. When only data from Barnett's Bank is assimilated, the state updates still result in an under-estimate of streamflow at Branch. As another example, consider the simulations at Wairau at Dip Flat. Assimilating data at Barnett's Bank increases the magnitude of the streamflow peaks at Dip Flat, but do not correct the timing errors. The timing errors at Dip Flat are not apparent at Barnett's Bank, so they are not corrected.

Fig. 5 (right column) shows a slight improvement in streamflow simulations at Barnett's Bank over the control run when data are

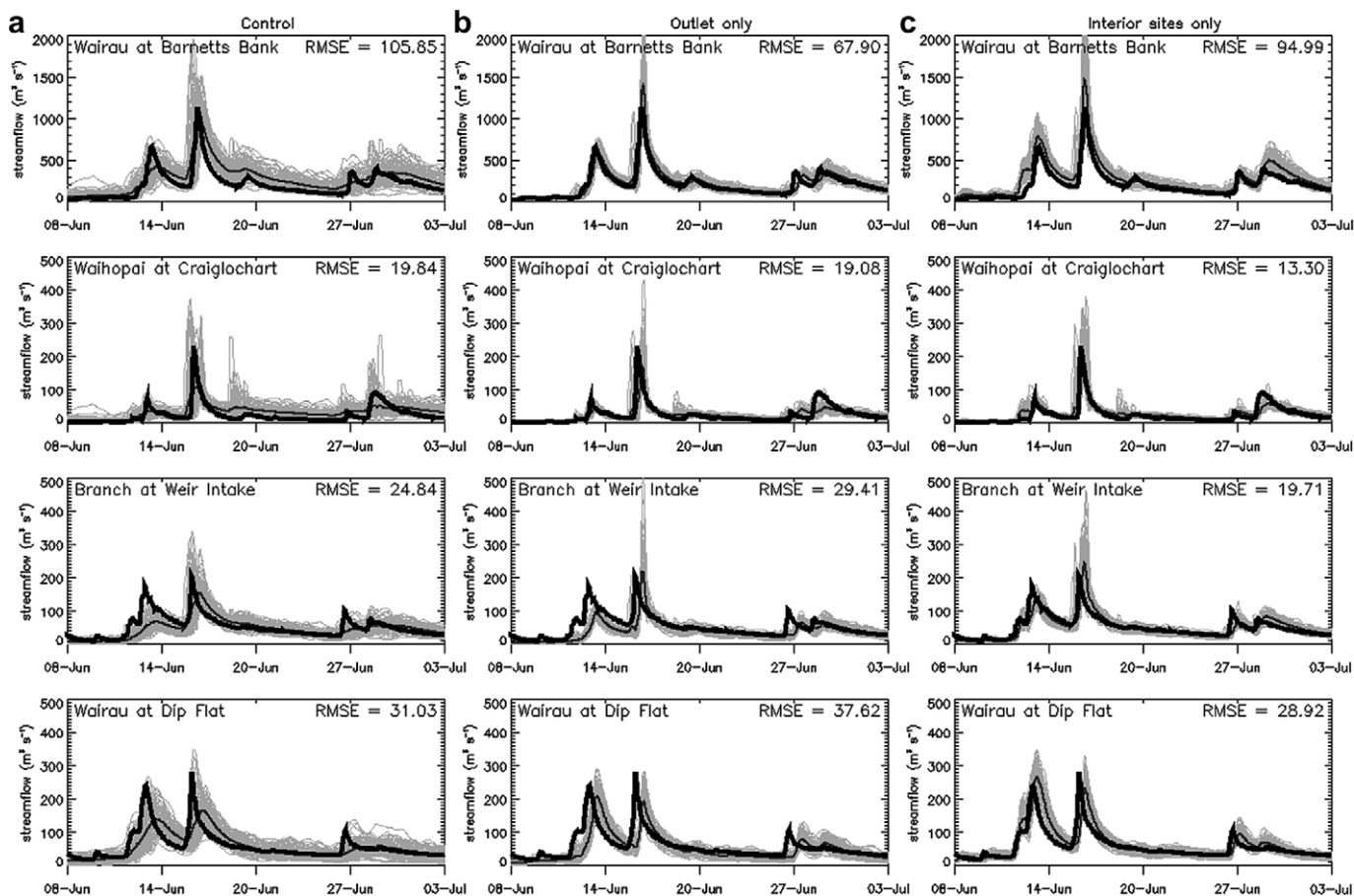


**Fig. 5.** Ensemble simulations for all four sites in the Wairau, showing (a) the control run (no data assimilation); (b) data only assimilated at the outlet (Barnetts Bank); and (c) data only assimilated at the interior locations (Waihopai at Craiglochart, Branch at Weir Intake, and Wairau at Dip Flat). The ensemble square root Kalman filter (EnSRF) is used for data assimilation. As in Fig. 3, the light grey lines are individual ensemble members, the grey line is the ensemble mean, and the thick black line is observations. See Fig. 2 for station locations.

assimilated at interior locations. However, streamflow simulations at Barnetts Bank are a little too high. This occurs because underestimates of streamflow are more pronounced at the interior locations than at Barnetts Bank, and only assimilating at interior locations results in state updates that are too large for the basin as a whole. Note that assimilating data at interior locations does improve streamflow simulations at the interior locations.

Another potential use of data assimilation is to transfer information from gauged to ungauged basins. To test this idea, simulations were performed when data was only assimilated at each of the three interior locations. Fig. 6 shows that while simulations do improve at the location where data are assimilated (compare the simulations in Fig. 6 with the control run in Fig. 5), simulations are degraded in all other locations.

The limited capability to propagate information between different basins is likely due to inadequacies in modelling the spatial variability of hydrological processes. Table 4 details correlations between time series of streamflow at each of the observing sites in the Wairau for the period 8th June–3rd July 2002, both for observations and model simulations. The modelled correlations are much higher than observed correlations for almost all station pairs. This indicates that state updates in distant locations may be too large.

Large spatial correlations in model output can occur due to insufficient spatial variability in model forcing and model parameters, or due to excessive correlation length scales used for model perturbations. The large spatial correlations are evident in both

the deterministic and the probabilistic model simulations (Table 4), which suggests there is insufficient variability in model forcings and parameters. Recall that spatially constant parameter multipliers are used to adjust *a priori* model parameter estimates in each sub-catchment. Some *a priori* model parameters are spatially uniform (for example, hydraulic conductivity, see Table 1), and other *a priori* model parameters may have insufficient spatial variability (for example, there can be considerable spatial variability in soil depth within a land resource inventory soil polygon, but this variability is not reflected in the mean soil depth value assigned to each sub-catchment). New parameter estimation methods are needed to produce *a priori* spatial fields of model parameters, and new calibration methods are needed to adjust the *a priori* parameter estimates so that model simulations have the correct spatial coherence.

## 8. Summary

This paper describes application of the ensemble Kalman filter (EnKF) in which streamflow observations are used to update states in a distributed hydrological model. We demonstrate that the standard implementation of the EnKF is inappropriate because of non-linear relationships between model states and observations. Transforming streamflow into log space before computing error covariances improves filter performance. We also demonstrate that model simulations improve when we use a variant of the EnKF

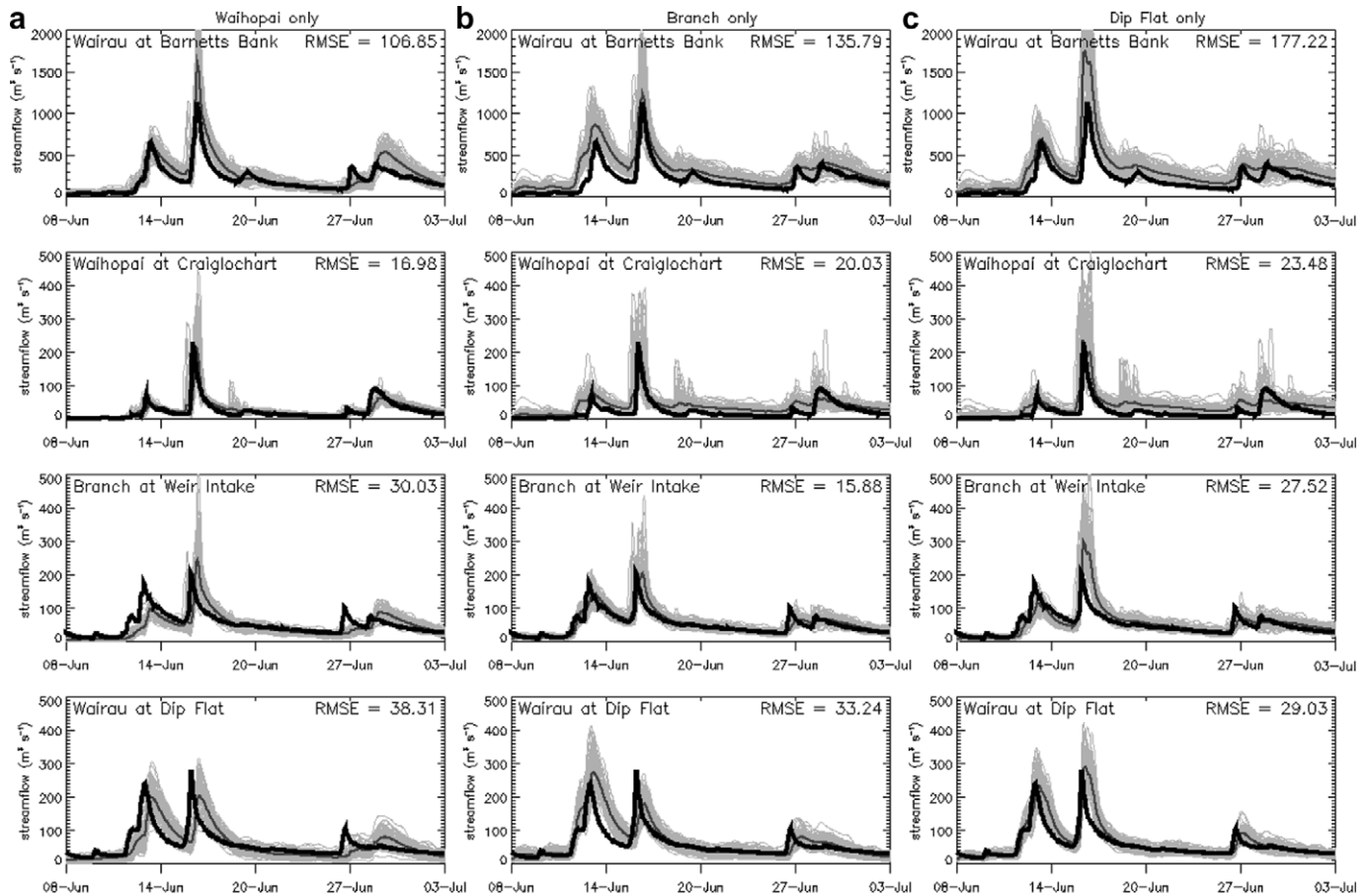


**Fig. 6.** Ensemble simulations for all four sites in the Wairau, showing (a) data only assimilated at the Waihopai at Craiglochchart; (b) data only assimilated at Branch at Weir Intake; and (c) data only assimilated at Wairau at Dip Flat. The ensemble square root Kalman filter (EnSRF) is used for data assimilation. As in previous figures, the light grey lines are individual ensemble members, the grey line is the ensemble mean, and the thick black line is observations. See Fig. 5 for control simulations and Fig. 2 for station locations.

**Table 4**  
Correlation of the time series between station pairs

Station pair	Observed	Deterministic simulation <sup>a</sup>	Model ensembles (0.05, 0.25, 0.50, 0.75, 0.95)
Wairau at Bannetts Bank vs. Waihopai at Craiglochchart	0.787	0.829	0.810, 0.843, 0.859, 0.876, 0.918
Wairau at Bannetts Bank vs. Branch at Weir Intake	0.706	0.988	0.941, 0.962, 0.971, 0.977, 0.982
Wairau at Bannetts Bank vs. Wairau at Dip Flat	0.601	0.831	0.740, 0.790, 0.847, 0.876, 0.916
Waihopai at Craiglochchart vs. Branch at Weir Intake	0.653	0.841	0.782, 0.850, 0.875, 0.896, 0.927
Waihopai at Craiglochchart vs. Wairau at Dip Flat	0.567	0.507	0.368, 0.506, 0.576, 0.623, 0.716
Branch at Weir Intake vs. Wairau at Dip Flat	0.955	0.832	0.735, 0.796, 0.837, 0.873, 0.910

<sup>a</sup> The deterministic simulation is where model inputs and states are not perturbed.

[44] that does not require perturbed observations. Our attempt to propagate information to neighbouring basins was unsuccessful, largely due to inadequacies in modelling the spatial variability of hydrological processes.

The methods for modelling model error in this paper are similar to those used in other studies (e.g., [33,42]), but are still simplistic

and subjective. They require specifying errors in model inputs and states, the decorrelation time, and correlation length scales. Reliable estimation of model errors is clearly critical – if error estimates are erroneous, then the model updates will be sub-optimal.

More rigorous methods for quantifying model error are needed. Examples are probabilistic precipitation estimation methods [10], and methods to construct ensembles of multiple models with different parameter sets and structure [7,12]. A necessary attribute of the “new” methods is the capability to adequately simulate the spatial correlation structure of model states and fluxes, as state updates in distant locations may be too large if the spatial correlation is too high. Spatial correlations are easily over-estimated if spatially constant parameter multipliers are used to adjust spatially uniform parameters (as is done in this study). New methods are required to establish spatially variable *a priori* parameter estimates, and new methods are required to adjust the *a priori* parameter estimates so that model simulations have the correct spatial coherence.

More attention should also be given to time lags between model states and streamflow. In this study the state updates are based on the instantaneous covariance between states and streamflow – this can reduce the optimality of the state updates. Pauwels and De Lannoy [45] recently introduced the bias-aware retrospective ensemble Kalman filter (REnKF) that explicitly accounts for time lags between model states and streamflow. They demonstrated with synthetic experiments that the bias-aware REnKF can correct for both errors in initial conditions and biases in precipitation data.

Accounting for the impact of time lags between states and streamflow is part of an ongoing research effort.

### Acknowledgements

We are grateful to Hoshin Gupta, M.S. Srinivasan and Greg Kelly for their valuable input, and we are indebted to three anonymous referees for their insightful comments. This research was funded by the New Zealand Foundation for Research Science and Technology (Contract C01X0401), the National Aeronautic and Space Administration (Contract NNG06GH10G), the National Oceanic and Atmospheric Administration (Contract NA06OAR4310065), and the National Weather Service Office of Hydrological Development (contract NWS4620014).

### Appendix A. The TopNet distributed hydrological model

The TopNet model has two fundamental components: (i) simulating the water balance over a number of sub-catchments throughout a river basin, and (ii) routing streamflow from each sub-catchment to the basin outlet.

#### A.1. State equations

There are five components of storage of water in a sub-catchment. They are the canopy storage ( $S_c$ ), snowpack storage ( $S_s$ ), soil, or root zone, storage ( $S_r$ ), aquifer storage ( $S_a$ ), and overland flow storage ( $S_o$ ). The movement of water in time  $t$  into and out of these storages is described by the following system of five differential equations

$$\begin{aligned} \frac{dS_c}{dt} &= p - p_t - e_c \\ \frac{dS_s}{dt} &= p_s - m_s \\ \frac{dS_r}{dt} &= i - e_r - d \\ \frac{dS_a}{dt} &= d - q_b \\ \frac{dS_o}{dt} &= q_{ix} + q_{sx} + q_b - q_o \end{aligned} \quad (A1)$$

The rate terms on the right-hand-side of each equation are defined below. For each discrete time step  $\Delta t$ , the individual equations in (A1) are solved in order from top to bottom, not simultaneously, taking advantage of analytical solutions where possible. This is done to greatly reduce computation time.

#### A.2. Canopy storage

The time rate of change in canopy storage is modelled following Ibbitt [20]. The canopy water state equation is

$$\frac{dS_c}{dt} = p - p_t - e_c \quad (A2a)$$

where  $p$  is the precipitation rate above the canopy,  $p_t$  is the rate of throughfall out of the canopy, and  $e_c$  is the rate of evaporation from the canopy. The precipitation rate  $p$  and the potential evaporation rate are used as model inputs, and throughfall  $p_t$  and canopy evaporation  $e_c$  are modelled as a quadratic function of canopy storage [20].

The rate of throughfall ( $p_t$ ) is calculated by

$$p_t = pf(S_c) \quad (A2b)$$

where

$$f(S_c) = \frac{S_c}{C_c} \left( 2 - \frac{S_c}{C_c} \right) \quad (A2c)$$

and  $C_c$  is the water holding capacity of the canopy. Physically,  $f(S_c)$  represents the fraction of leaf area that is wet, relative to its maximum. Eqs. (A2b) and (A2c) signify that less precipitation is added to canopy storage ( $S_c$ ) – that is, there is more throughfall – as the canopy reaches its capacity ( $C_c$ ).

Canopy evaporation ( $e_c$ ) is calculated as

$$e_c = e_{\text{pot}} c_r f(S_c) \quad (A2d)$$

where  $c_r$  is a parameter used to quantify higher evaporation losses from interception relative to the potential evapotranspiration rate  $e_{\text{pot}}$ . The potential evaporation rate  $e_{\text{pot}}$  is computed using the Priestley–Taylor method [30], with radiation terms estimated empirically using the methods in Shuttleworth [39].

#### A.3. Snow storage

The rate of change of snow water equivalent storage is given by

$$\frac{dS_s}{dt} = p_s - m_s \quad (A3)$$

where  $p_s$  is the snow throughfall rate through the canopy and  $m_s$  the snow melt rate. TopNet has several options for determining the rates of snow accumulation and melt, but are not discussed here because snow has a limited impact on the hydrology of the basin examined in this study.

#### A.4. Soil storage

The basic soil or root zone state equation is

$$\frac{dS_r}{dt} = i - e_r - d \quad (A4a)$$

where  $i$  is the infiltration rate,  $e_r$  is the soil evaporation rate, and  $d$  is the rate of drainage from the soil to the aquifer.

##### A.4.1. Infiltration

The infiltration rate  $i$  into the soil layer is limited by the canopy throughfall rate  $p_t$  minus the evaporation rate of the throughfall  $e_t$ , and the maximum infiltration rate  $i_{\text{max}}$ :

$$i = \min[i_{\text{max}}, p_t - e_t] \quad (A4b)$$

where the evaporation from throughfall is determined by the potential evaporative demand, i.e.,  $e_{\text{pot}} - e_c$ , not met by the canopy evaporation:

$$e_t = \min[e_{\text{pot}} - e_c, p_t] \quad (A4c)$$

The maximum infiltration rate is modelled using a Green–Ampt formulation

$$i_{\text{max}} = K_0 e^{-z_f/m} \frac{z_f + \psi_f}{z_f} \quad z_f < z_r \quad (A4d)$$

where  $\psi_f$  is the Green–Ampt wetting front suction,  $z_f$  is the depth of the wetting front and  $z_r$  is the soil depth. The parameters  $K_0$  and  $m$  define the vertical saturated hydraulic conductivity profile of the subsurface. When  $z_f$  reaches  $z_r$ , the soil is completely saturated and  $i_{\text{max}} = 0$ . The depth to the wetting front is approximated by

$$z_f = \frac{S_r}{\theta_{\text{sat}}} \quad (A4e)$$

where  $S_r = \theta z_r$ , and  $\theta$  and  $\theta_{\text{sat}}$  are the relative soil water contents at actual and saturated conditions, respectively.

##### A.4.2. Soil evaporation

Evaporation from the soil  $e_r$  is driven by the potential evaporative demand not met by either the canopy or throughfall evapora-

tion, or  $e_{pot} - (e_c + e_t)$ . Furthermore,  $e_r$  is a function of the relative water content  $\theta$

$$e_r = (e_{pot} - e_c - e_t) \min\left(\frac{\theta}{\theta_{pa}}, 1\right) \quad (A4f)$$

where  $\theta_{pa}$  is the plant-available relative water content when the plant-available water storage is saturated. Thus, for  $\theta < \theta_{pa}$ ,  $e_r$  decreases linearly to zero as the soil moisture approaches zero.

#### A.4.3. Drainage

The drainage rate  $d$  is a power function of the relative soil water content and is given by

$$d = K_r \theta^c \quad (A4g)$$

where  $K_r$  is the saturated hydraulic conductivity at  $z_r$  (the bottom of the soil layer) and the exponent  $c$  is a function of the unsaturated hydraulic properties of the soil. The value of  $K_r$  is calculated as

$$K_r = K_0 e^{-z_r/m} \quad (A4h)$$

#### A.4.4. Sub-grid variability and surface water–groundwater interactions

Eqs. (A4a–h) are only strictly valid for cases where the depth to the water table is lower than the depth of the soil layer (Fig. 1). TopNet uses TOPMODEL concepts to simulate sub-grid variability in the depth to the water table [5,6]. TopNet includes the option of using the original exponential subsurface transmissivity relationship in TOPMODEL [5], or a power-law representation for transmissivity [1,15,22,35]. Here we only express the TopNet model equations as they relate to the exponential transmissivity function because that is the one used in this study.

In TopNet, a catchment area is divided into three zones based on the local depth of the water table with respect to the ground surface and the bottom of the soil layer. In areas where the water table is below the bottom of the soil layer, the catchment soil layer is “uninfluenced” by the local water table. In areas where the water table lies between the soil surface and the bottom of the soil layer, the soil layer is “influenced” by the water table. Lastly, in areas where the water table is at or above the soil surface, the soil is “saturated” (see Fig. 1).

The local depth to the water table  $z$  is computed directly from the local topographic index,  $a/\tan\beta$ , where  $a$  is the area per unit contour width draining through a given point from upslope, and  $\tan\beta$  is the local slope. Areas with high index values indicate areas of topographic convergence and areas that tend to saturate first. The local depth to the water table is

$$z = \bar{z} + m[\lambda - \ln(a/\tan\beta)] \quad (A4i)$$

where  $\bar{z}$  is the sub-catchment spatial average of the depth to the water table,  $m$  is a depth scaling parameter, and  $\lambda$  is the spatial average of the transformed topographic indices  $\ln(a/\tan\beta)$

$$\lambda = \frac{1}{A} \int_A \ln(a/\tan\beta) \quad (A4j)$$

where  $A$  is the sub-catchment area.

The fractional area of the saturated zone  $\phi_{sat}$  is determined from the soil parameters and the cumulative distribution function (CDF) of the transformed topographic index  $\kappa$ , given by  $\ln(a/\tan\beta)$ , such that

$$\phi_{sat} = \text{Prob}(\kappa > \kappa_{sat}) = 1 - \text{CDF}(\kappa_{sat}) \quad (A4k)$$

where  $\kappa_{sat}$  is calculated by

$$\kappa_{sat} = \frac{\bar{z}}{m} + \lambda \quad (A4l)$$

The fractional area of the uninfluenced zone  $\phi_{unf}$  is determined similarly, but accounts for the depth of the soil layer. The fractional area is given by

$$\phi_{unf} = \text{Prob}(\kappa < \kappa_{unf}) = \text{CDF}(\kappa_{unf}) \quad (A4m)$$

where  $\kappa_{unf}$  is calculated by

$$\kappa_{unf} = \frac{\bar{z} - z_r}{m} + \lambda \quad (A4n)$$

The fractional area of the influenced zone  $\phi_{inf}$  is simply  $1 - \phi_{sat} - \phi_{unf}$ .

The fractions of the catchment that are “saturated”, “influenced” and “uninfluenced” (i.e.,  $\phi_{sat}$ ,  $\phi_{inf}$ , and  $\phi_{unf}$ ) defines the interaction of the water table with the soil zone, and the fluxes in Eq. (A4a) are modified to account for the “extra” water in the soil layer. This is formalized as follows. Let  $S_r$  be the sum of the soil water in each zone such that

$$S_r = S_{unf} + S_{inf} + S_{sat} \quad (A4o)$$

where the subscripts unf, inf, and sat denote the uninfluenced, influenced, and saturated zones, respectively. The change in soil water is then the sum of the change in soil moisture in each zone:

$$\frac{dS_r}{dt} = \frac{dS_{unf}}{dt} + \frac{dS_{inf}}{dt} + \frac{dS_{sat}}{dt} \quad (A4p)$$

The soil layer state equation can be expressed more fully as

$$\begin{aligned} \frac{dS_r}{dt} = & \phi_{unf}(i_{unf} - e_{unf} - d_{unf}) + \phi_{inf}(i_{inf} - e_{inf} - d_{inf}) \\ & + \phi_{sat}(-e_{sat} - d_{sat}) \end{aligned} \quad (A4q)$$

where  $\phi_{unf}$ ,  $\phi_{inf}$ , and  $\phi_{sat}$  represent the fractional areas of the catchment that are uninfluenced, influenced, and saturated, respectively, and the other terms are as given in (A4a) but subscripted to denote to which zone they pertain. For convenience, we impose the condition that the relative change in soil moisture storage is the same across all zones, such that

$$\frac{dS_r}{dt} = \frac{1}{\phi_{unf}} \frac{dS_{unf}}{dt} = \frac{1}{\phi_{inf}} \frac{dS_{inf}}{dt} = \frac{1}{\phi_{sat}} \frac{dS_{sat}}{dt} \quad (A4r)$$

The rates in the state equation for the uninfluenced zone (i.e., the first set of terms on the right-hand-side of Eq. (A4q)) are computed using Eqs. (A4b) through (A4h) with the following substitutions:  $i_{unf}$  for  $i$ ,  $e_{unf}$  for  $e_r$ ,  $d_{unf}$  for  $d$ , and  $S_{unf}$  for  $S_r$ .

The state equation for the influenced zone (i.e., the second set of terms on the right-hand-side of Eq. (A4q)) is adjusted to account for the presence of the water table within the soil layer. The value of  $S_{inf}$  is computed as a weighted average of the saturated and unsaturated portions of the soil column:

$$S_{inf} = S_{unf} \frac{z}{z_r} + z_r \theta_{sat} \frac{z_r - z}{z_r} \quad (A4s)$$

The uninfluenced soil zone rate Eqs. (A4b) through (A4h) are also used to compute infiltration and evaporation, substituting  $i_{inf}$  and  $e_{inf}$  for  $i$  and  $e_r$ , respectively. However, the adjusted soil moisture for the influenced zone is  $\theta = S_{inf}/z_r$  and adjusted wetting front depth is  $z_f = S_{inf}/\theta_{sat}$ . Unlike infiltration and evaporation, the drainage  $d_{inf}$  is determined from the equality in (A4r), hence

$$i_{unf} - e_{unf} - d_{unf} = i_{inf} - e_{inf} - d_{inf} \quad (A4t)$$

When forcing is positive, or evaporation is zero, (A4q) may be solved for  $d_{inf}$  as

$$d_{inf} = d_{unf} - i_{unf} + i_{inf} \quad (A4u)$$

on condition that  $d_{inf} \geq 0$ . Otherwise  $d_{inf} = 0$ . When forcing is negative, or infiltration is zero, (A4t) becomes

$$d_{inf} = d_{unf} + e_{unf} - e_{inf} \quad (A4v)$$

In the saturated zone we assume there is no infiltration (i.e., all inputs are saturation excess runoff). Because the soil layer is saturated, evaporation from the soil is not soil-moisture limited, thus  $e_{sat}$  is given by

$$e_{sat} = [e_{pot} - (e_c + e_t)] \tag{A4w}$$

Similar to the influenced zone drainage, the saturated zone drainage  $d_{sat}$  is determined from the equality in (A4r), hence

$$i_{unf} - e_{unf} - d_{unf} = -e_{sat} - d_{sat} \tag{A4x}$$

When forcing is positive, or evaporation is zero, (A4x) may be solved for  $d_{sat}$  as

$$d_{sat} = d_{unf} - i_{unf} \tag{A4y}$$

on condition that  $d_{sat} \geq 0$ . Otherwise  $d_{sat} = 0$ . When forcing is negative, or infiltration is zero, (A4x) becomes

$$d_{sat} = d_{unf} + e_{unf} - e_{sat} \tag{A4z}$$

### A.5. Aquifer storage

The groundwater state equation in (A1) can be rewritten as

$$-\theta_{dr} \frac{dz}{dt} = d - q_b \tag{A5a}$$

where  $q_b$  is the aquifer discharge rate, or rate of baseflow. In (A5a) the change in aquifer or groundwater storage is set equal to the change in the basin average water table depth  $\bar{z}$  times the drainable water content  $\theta_{dr}$ .

The drainage rate is the sum of the drainage from each of the soil zones, or

$$d = \phi_{unf} d_{unf} + \phi_{inf} d_{inf} + \phi_{sat} d_{sat} \tag{A5b}$$

The baseflow rate is calculated by the following:

$$q_b = K_0 m e^{-\lambda} e^{-\bar{z}/m} \tag{A5c}$$

where all the terms are as defined previously.

### A.6. Surface storage

Surface runoff generated from a basin will be delayed as it travels overland before reaching the river network, resulting in a basin surface storage. The overland flow pathways include hillslope surfaces and transient and therefore unresolved stream channels. Surface runoff, or basin outflow, can be generated in three ways: as infiltration-excess runoff  $q_{ix}$ , saturation-excess runoff  $q_{sx}$ , or as subsurface discharge  $q_b$ . The state equation for surface storage is

$$\frac{dS_o}{dt} = q_{ix} + q_{sx} + q_b - q_o \tag{A6a}$$

where  $q_o$  is the basin outflow from the surface storage to the river network. It is assumed that all three sources of basin discharge (infiltration-excess, saturation-excess, and subsurface discharge) enter the surface store before entering the river network.

Infiltration-excess runoff  $q_{ix}$  occurs in the uninfluenced and influenced portions of the catchment when the forcing exceeds the infiltration rate. The infiltration-excess runoff rate is calculated for any point as

$$q_{ix} = \max(p_t - e_t - i, 0) \tag{A6b}$$

However, the infiltration rates may differ for the uninfluenced and influenced zones due to the differing soil water contents in each zone (see Section A.4), resulting in distinct infiltration-excess runoff rates from each zone. The fractional area-weighted infiltration-excess runoff is calculated as

$$q_{ix} = \phi_{unf} q_{ix,unf} + \phi_{inf} q_{ix,inf} \tag{A6c}$$

where  $q_{ix,unf}$  and  $q_{ix,inf}$  are the infiltration-excess runoff rates from the uninfluenced and influenced zones, respectively.

Saturation-excess runoff occurs in the saturated portion of the catchment when forcing is positive. The infiltration is set to zero and the saturation-excess runoff rate is calculated by

$$q_{sx} = \max[\phi_{sat}(p_t - e_t), 0] \tag{A6d}$$

The basin discharge  $q_o$  is subject to a time delay, where the delay is computed using the frequency distribution of overland flow residence time  $\tau$ . The residence time distribution  $f(\tau)$  is calculated for each basin as the empirical frequency distribution of overland path lengths  $x$  divided by a constant overland flow velocity  $v$ : i.e.,  $f(\tau) = f(x/v)$ .

The surface storage in time is calculated by tracking the volume of water associated with each residence time  $\tau$ . Let  $dV(\tau) = M(\tau)d\tau$  be an infinitesimal volume of surface water existing at some time  $t$  that is destined to leave the surface of the basin after some time  $\tau$  has elapsed, where  $M$  is the rate of change in volume with respect to  $\tau$ . The total basin surface storage at time  $t$  across all  $\tau$  is

$$S_o = \int_0^\infty M(\tau) d\tau \tag{A6e}$$

The change in  $dV(\tau)$  with time is given by

$$\frac{d}{dt} [dV(\tau)] = q_{in}(\tau) - q_{out}(\tau) \tag{A6f}$$

where  $q_{in}(\tau)$  and  $q_{out}(\tau)$  are the inflow to, and outflow from, the volume of water with residence time  $\tau$ . The inflow is partly composed of the various sources of surface water runoff, which are weighted by the frequency distribution of residence times  $f(\tau)$ . The remaining inflow comes from the volume of water with residence time  $\tau + dt$ :

$$q_{in}(\tau) = (q_{ix} + q_{sx} + q_b) f(\tau) + \frac{dV(\tau + dt)}{dt} \tag{A6g}$$

The outflow over  $dt$  is simply the volume of water with residence time  $\tau$ :

$$q_{out}(\tau) = \frac{dV(\tau)}{dt} \tag{A6h}$$

The outflow rate from the basin into the river network is

$$q_o = \frac{dV(\tau = 0)}{dt} \tag{A6i}$$

In practice, the residence time distribution  $f(\tau)$  is discretized and the interval size  $\Delta\tau$  is equal to the simulation time step, i.e.,  $\Delta\tau = \Delta t$ . Eq. (A6f) is solved for each discrete value of  $\tau \geq 0$  up to some predefined maximum value of  $\tau$ .

The surface storage is illustrated graphically in Fig. A1. The top plot shows for an example sub-catchment both the cumulative probability distribution of distance to the stream (meters), and the corresponding probability distribution of travel times (seconds), obtained by  $f(\tau) = f(x/v)$ . Here the probability distribution of travel times is discretized into hourly time steps. The bottom three plots in Fig. A1 show respectively example inflow ( $q_{ix} + q_{sx} + q_b$ ), storage ( $S_o$ ) for time  $\tau = 5$ , and basin discharge ( $q_o$ ), as computed using Eqs. (A6e) through (A6i). Note the delay between the inflow ( $q_{ix} + q_{sx} + q_b$ ) and outflow ( $q_o$ ) time series.

### A.7. Flow routing through the river network

Flow routing in TopNet is modelled using a one-dimensional Lagrangian kinematic wave routing scheme, in which runoff produced by each sub-catchment is propagated as “particles” through the stream network to the basin outlet.

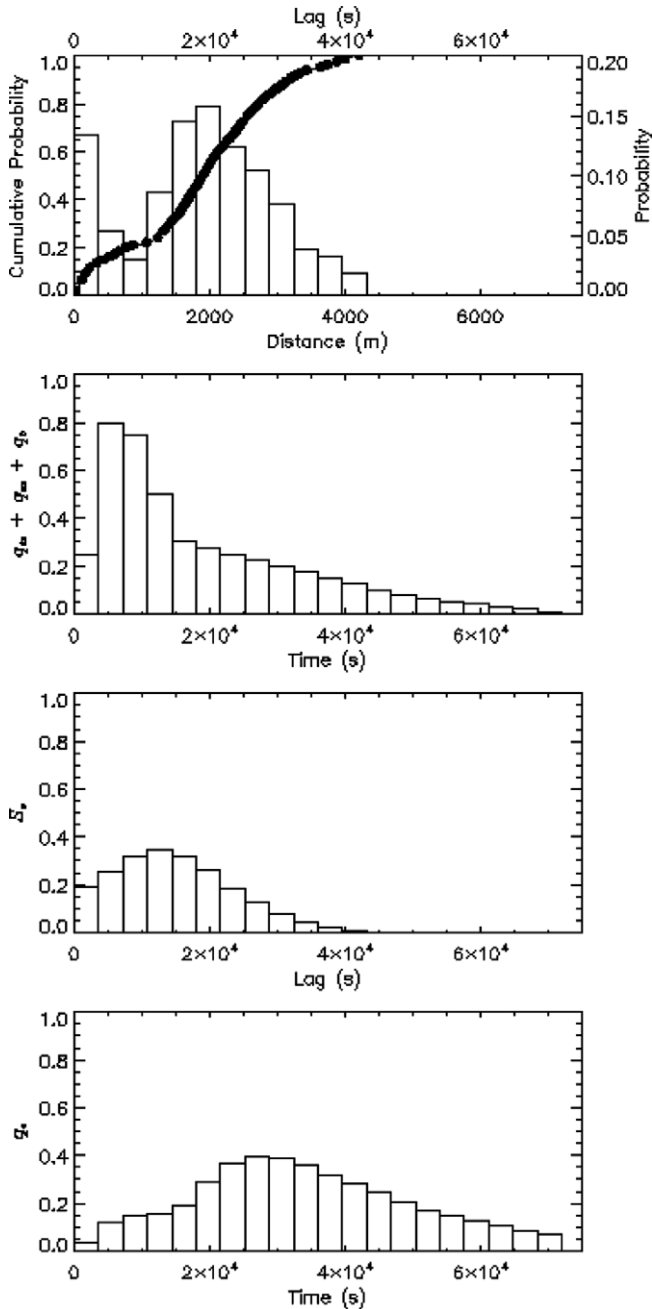


**Fig. A1.** Depiction of the time delay of runoff through the transient and therefore unresolved stream network in headwater river basins. The top plot shows the cumulative probability distribution of the distance to the stream and the corresponding probability distribution of travel times (seconds), obtained by  $f(\tau) = f(x/v)$ . The bottom three plots show respectively example inflow ( $q_{ia} + q_{sa} + q_b$ ), a snapshot of storage ( $S_0$ ) for time  $t = 5$ , and basin discharge ( $q_a$ ), as computed using Eqs. (A6e) through (A6i).

We assume the channel is hydraulically wide, and that the water level depth ( $y$ ) is a good approximation for the area of the channel. Given Manning’s stage-discharge relationship

$$q = \frac{\sqrt{S}}{N} y^\alpha \tag{A7a}$$

where  $S$  is the channel slope,  $N$  is Manning’s  $n$ , and  $\alpha$  is a parameter ( $5/3$ ), the particle celerity  $v$  is

$$v = \frac{dq}{dy} = \alpha \left( \frac{\sqrt{S}}{N} \right)^{\frac{1}{2}} q^{\left( \frac{\alpha-1}{\alpha} \right)} \tag{A7b}$$

and the travel time for an individual flow particle over the length of a channel segment,  $\tau$ , is

$$\tau = \frac{L}{v} \tag{A7c}$$

where  $L$  is the length of the channel segment.

Time is used for particle tracking in the following way. In a given channel segment we have knowledge of the time a flow particle entered that segment, and, based on the estimated travel time (Eq. (A7c)), we have knowledge of the time that the flow particle is expected to exit the segment. If the particle is computed to exit the segment before the end of the time step, then that particle is flagged as “routed” and is moved to the downstream river segment. Otherwise, the flow particle is flagged as “non-routed”, and remains in the given channel segment. In this context earlier entry times imply that a flow particle is nearer to the end of a channel segment.

A special (but common) case occurs on the rising limb of the hydrograph, where faster particles merge with slower particles to form a discontinuity known as a kinematic shock. When this occurs, flow particles on either side of the discontinuity are merged and assumed to travel at the same celerity [48].

Our network implementation of the Lagrangian routing model requires merging flow from multiple upstream reaches. This is complicated because particles from different upstream reaches enter the downstream reach at different times. For each particle that exits one of the upstream reaches, we create a new particle at the same time in all of the other upstream reaches. The particle injected into the downstream reach is then equal to the particle that exited an upstream reach plus the sum of the new particles in all of the other upstream reaches. The new particles in a given upstream reach are produced by linearly interpolating between the last particle that exited that reach and the particles that are still in that reach.

The state variables in the river network are therefore all times and flows of the individual particles, and timestep-average streamflow for each reach in the stream network is the weighted average of all particles that exit a reach in a given time step. Timestep-average streamflow is therefore a diagnostic variable, not a state variable.

**References**

- [1] Ambrose B, Beven K, Freer J. Toward a generalization of the TOPMODEL concepts: topographic indices of hydrological similarity. *Water Resour Res* 1996;32:2135–45.
- [2] Arulampalam MS, Maskell S, Gordon N, Clapp T. A tutorial on particle filters for online nonlinear/non-Gaussian Bayesian tracking. *IEEE Trans Signal Process* 2002;50:174–88.
- [3] Bandaragoda C, Tarboton DG, Woods RA. Application of TOPNET in the distributed model intercomparison project. *J Hydrol* 2004;298:178–201.
- [4] Bartholmes J, Todini E. Coupling meteorological and hydrological models for flood forecasting. *Hydrol Earth Syst Sci* 2005;9:333–46.
- [5] Beven KJ, Kirkby RJ. A physically based variable contributing area model of basin hydrology. *Hydrol Sci Bull* 1979;43–69.
- [6] Beven K. TOPMODEL: a critique. *Hydrol Process* 1997;11:1069–85.
- [7] Beven KJ. A manifesto for the equifinality thesis. *J Hydrol* 2006;320:18–36.
- [8] Burgers G, van Leeuwen PJ, Evensen G. Analysis scheme in the ensemble Kalman filter. *Mon Weather Rev* 1998;126:1719–24.
- [9] Clark MP, Hay LE. Use of medium-range numerical weather prediction model output to produce forecasts of streamflow. *J Hydrometeorol* 2004;5:15–32.
- [10] Clark MP, Slater AG. Probabilistic quantitative precipitation estimation in complex terrain. *J Hydrometeorol* 2006;7:3–22.
- [11] Clark MP, Ibbitt RP, Woods RA. Flood forecasts for New Zealand communities. *Water Atmosph* 2007;15(3):14–5.
- [12] Clark MP, Slater AG, Rupp DE, Woods RA, Vrugt JA, Gupta HV, et al. The Framework for Understanding Structural Errors (FUSE): a modular framework to diagnose differences between hydrological models. *Water Resour Res* 2008. doi:10.1029/2007WR006735 [in press, accepted 12 May 2008].
- [13] Crow WT, van Loon E. Impact of incorrect model error assumptions on the sequential assimilation of remotely sensed soil moisture. *J Hydrometeorol* 2006;7:421–32.

- [14] De Roo APJ et al. Development of a European flood forecasting system. *Int J River Basin Manage* 2003;1(1):49–59.
- [15] Duan JF, Miller NL. A generalized power function for the subsurface transmissivity profile in TOPMODEL. *Water Resour Res* 1997;33:2559–62.
- [16] Evensen G. Using the extended Kalman filter with a multi-layer quasi-geostrophic ocean model. *J Geophys Res* 1992;97:17905–24.
- [17] Evensen G. Sequential data assimilation with a nonlinear quasi-geostrophic model using Monte Carlo methods to forecast error statistics. *J Geophys Res* 1994;99:10143–62.
- [18] Evensen G. The ensemble Kalman filter: theoretical formulation and practical implementation. *Ocean Dynam* 2003;53:343–67.
- [19] Gouweleeuw BT, Thielen J, Franchello G, De Roo APJ, Buizza R. Flood forecasting using medium-range probabilistic prediction. *Hydrol Earth Syst Sci* 2005;9:365–80.
- [20] Ibbitt R. Development of a conceptual model of interception. Unpublished Hydrological Research Progress Report No. 5, Ministry of Works, New Zealand, 1971.
- [21] Ibbitt R, Thompson C, Turner R. Skill assessment of a linked precipitation-runoff flood forecasting system. *J Hydrol (NZ)* 2005;44:91–104.
- [22] Iorgulescu I, Musy A. Generalization of TOPMODEL for a power law transmissivity profile. *Hydrol Process* 1997;11:1353–5.
- [23] Kitinadis PK, Bras RL. Real time forecasting with a conceptual hydrologic model. 1. Analysis of uncertainty. *Water Resour Res* 1980;16:1025–33.
- [24] Kitinadis PK, Bras RL. Real time forecasting with a conceptual hydrologic model. 2. Applications and results. *Water Resour Res* 1980;16:1034–44.
- [25] Liu Y, Gupta HV. Uncertainty in hydrologic modeling: toward an integrated data assimilation framework. *Water Resour Res* 2007;43. doi:10.1029/2006WR005756. W07401.
- [26] Miller RN, Ghil M, Ghautiez F. Advanced data assimilation in strongly nonlinear dynamical systems. *J Atmosph Sci* 1994;51:1037–55.
- [27] Moradkhani H, Hsu K, Gupta HV, Sorooshian S. Uncertainty assessment of hydrologic model states and parameters: sequential data assimilation using the particle filter. *Water Resour Res* 2005;41. doi:10.1029/2004WR003604. W05012.
- [28] Newsome PFJ, Wilde RH, Willoughby EJ. Land resource information system spatial data layers. Technical Report, Palmerston North, New Zealand, Landcare Research NZ Ltd, 2000.
- [29] Pham DT. Stochastic methods for sequential data assimilation in strongly nonlinear systems. *Mon Weather Rev* 2001;129:1194–207.
- [30] Priestley CHB, Taylor RJ. On the assessment of surface evaporation using large-scale parameters. *Mon Weather Rev* 1972;100:81–92.
- [31] Reed S, Koren V, Smith M, Zhang Z, Moreda F, Seo DJ. Overall distributed model intercomparison project results. *J Hydrol* 2004;298:27–60.
- [32] Reichle RH, Entekhabi D, McLaughlin DB. Downscaling of radiobrightness measurements for soil moisture estimation: a four-dimensional variational data assimilation approach. *Water Resour Res* 2001;37:2353–64.
- [33] Reichle RH, Walker JP, Koster RD, Houser PR. Extended versus ensemble Kalman filtering for land data assimilation. *J Hydrometeorol* 2002;3:728–40.
- [34] Reichle RL, Koster RD. Assessing the impact of horizontal error correlations in background fields on soil moisture estimation. *J Hydrometeorol* 2003;4:1229–42.
- [35] Rupp DE, Woods RA. Increased flexibility in base flow modelling using a power law transmissivity profile. *Hydrol Process* 2008;22:2667–71.
- [36] Seo DJ, Koren V, Cajina N. Real-time variational assimilation of hydrologic and hydrometeorological data into operational hydrologic forecasting. *J Hydrometeorol* 2003;4:627–41.
- [37] Snelder TH, Biggs BJF. Multi-scale river environment classification for water resources management. *J Am Water Resour Assoc* 2002;38:1225–40.
- [38] Sorooshian S, Dracup JA. Stochastic parameter estimation procedures for hydrologic rainfall-runoff models: Correlated and heteroscedastic error cases. *Water Resour Res* 1980;16:430–42.
- [39] Shuttleworth WJ. Evaporation. In: Maidment DR, editor. *Handbook of hydrology*. New York: McGraw-Hill; 1993 [chapter 4].
- [40] Tait AB, Henderson RD, Turner RW, Zheng X. Thin plate smoothing spline interpolation of daily rainfall for New Zealand using a climatological rainfall surface. *Int J Climatol* 2006;2097–115.
- [41] Tolson BA, Shoemaker CA. Dynamically dimensioned search algorithm for computationally efficient watershed model calibration. *Water Resour Res* 2007;43. doi:10.1029/2005WR004723. W01413.
- [42] Vrugt JA, Gupta HV, Nualláin BÓ, Bouten W. Real-time data assimilation for operational ensemble streamflow forecasting. *J Hydrometeorol* 2006;7:548–65.
- [43] Weerts AH, El Serafy GYH. Particle filtering and ensemble Kalman filtering for state updating with hydrological conceptual rainfall-runoff models. *Water Resour Res* 2006;42. doi:10.1029/2005WR004093. W09403.
- [44] Whitaker JS, Hamill TM. Ensemble data assimilation without perturbed observations. *Mon Weather Rev* 2002;130:1913–24.
- [45] Pauwels RN, De Lannoy JM. Improvement of modeled soil wetness conditions and turbulent fluxes through the assimilation of observed discharge. *J Hydrometeorol* 2006;7:458–77.
- [46] Georgakakos KP. A generalized stochastic hydrological model for flood and flash-flood forecasting: 1. Formulation. *Water Resour Res* 1986;22:2083–95.
- [47] Georgakakos KP. A generalized stochastic hydrological model for flood and flash-flood forecasting: 2. Case studies. *Water Resour Res* 1986;22:2096–106.
- [48] Goring DG. Kinematic shocks and monoclinal waves in the Waimakariri, a steep, braided, gravel-bed river. In: *Proceedings of the International Symposium on waves: Physical and numerical modelling*, University of British Columbia, Vancouver, Canada, 1994, p. 336–45.